LABORATORI NAZIONALI DI FRASCATI
SIS – Pubblicazioni

LNF-02/009 (P)
10 Maggio 2002

PROBING THE COORDINATION AND GEOMETRY OF HEME-IRON LIGANDS IN HEMOPROTEINS BY XANES (X-RAY ABSORPTION NEAR EDGE STRUCTURE)

M. Benfatto
Laboratori Nazionali di Frascati dell'INFN, C.P.13 - 00044 Frascati, Italy

S. Della Longa
Dip. Medicina Sperimentale, Univ. L' Aquila (Italy) via Vetoio, loc. Coppito II, L' Aquila Italy
and Laboratori Nazionali di Frascati dell'INFN, C.P.13 - 00044 Frascati, Italy

Abstract

X-ray Absorption Near Edge Structure (XANES) spectroscopy, is an emerging technique related to EXAFS (Extended X-ray Absorption Fine Structure) spectroscopy. XANES probes the electronic state and the atomic structure of a metal site in biological macromolecules at any physical state of the sample and any environmental condition. For instance, the pH-dependent and temperature-dependent XANES spectra of ferric aquomet-myoglobin in solution have been studied to probe the main Fe-heme conformational changes following its acid-alkaline chemical transition, and the temperature-dependent spin transition of the alkaline form.

In these last years, multiple scattering (MS) theory has been shown able to reproduce satisfactorily the experimental XANES data from the edge up to 150-200 eV. The ability to analyse the low-energy part of a x-ray absorption spectrum allows determining structural data that are very difficult to recover by EXAFS, such as bonding angles.

Using light triggered systems allows studying trapped intermediate conformations and some aspects of the dynamics of biological complexes. XANES theory has been applied to interpret the dramatic spectroscopical changes in the XANES spectrum of a carbonmonoxy-myoglobin single crystal, following the photolysis of the Fe-CO bond at T=20K. The distance and orientation of the CO molecule from the Fe atom, and the position of the proximal histidine, have been determined at a resolution comparable with that of the more recent X-ray diffraction (XRD) studies. Preliminary applications of the quantitative XANES analysis to hemoproteins in solutions are also presented

Running title: XANES of hemoproteins

Submitted to Transword Research Network

1. INTRODUCTION

A deeper understanding of the function and the catalytic mechanism of hemoproteins is based on the characterization of the coordination state of the heme iron. The accurate determination of the binding geometry of the iron 5th and 6th ligand is important as it is strongly linked to both the electronic state of the iron and the protein function. It is difficult, however, to extract unambiguous information on the axial coordination of the heme iron from non-crystalline samples. In facts, UV/V spectroscopy is very sensitive to the heme π electron density, but is poorly sensitive to the axial symmetry; the structural interpretation of temperature dependent data is even more complicated because of strong vibrational coupling [1]. Electron Paramagnetic Spectroscopy (EPR) can reveal structural details only at low temperature [2]. Resonance Raman Spectroscopy is very sensistive to the Fe-heme arrangement but the 5th and 6th iron ligand geometries remain elusive: a Fe-His stretching vibration has been assigned unambiguously only in deoxy-myoglobin (at ~220 cm^{-1}); a Resonance Raman peak (in the range 490-500 cm^{-1}) has been assigned to the Fe-O stretching frequency in aquomet-myoglobin [3]: the observed 5 cm^{-1} shift between alkalin aquomet-hemoglobin (Hb^+OH^-, 495 cm^{-1}) and myoglobin (Mb^+OH^-, 490 cm^{-1}) was interpreted as due to a Fe-O bond length increasing of only 0.01 Å, but the correlation between Raman frequency shifts and bond length changes are questioned.

Even when X-ray diffraction (XRD) data are available, some ambiguities remain on the Fe axial ligand coordination. One example has been given in the case of the low temperature photoproduct of carbonmonoxy-myoglobin: an unligated [4], or a partially CO ligated [5] Fe-heme are reported at 40K; different results are found depending on the way by which the electron density map is analysed, with or without a Fe-6th ligand distance restrain. Moreover XRD does not probe the redox state of the iron, and it is difficult to apply XRD studies to study redox-linked conformational changes, effects due to pH, solvent, allosteric factors, and so on.

The advent of the use of Synchrotron Radiation (SR) [6,7] has given a tremendous impulse to the areas of research using X-ray. It has allowed determining by XRD protein structures at atomic resolution [8] where C-C bonds are visible. X-ray Absorption Spectroscopy (XAS) is another SR technique [9,10], including both XANES (X-ray Absorption Near Edge Structure) spectroscopy, that studies an X-ray absorption edge up to the first 50-100 eV, and EXAFS (Extended X-ray Absorption Fine Structure) spectroscopy, analysing the extended energy region above the edge, from about 50-100 eV to an energy limited from the signal-to-noise ratio of the collected data. The unique properties of SR sources, like tunability, brilliance, intensity and polarization, to cite few, make the XAS a unique tool for the investigation of the geometrical and electronic structure of many systems from biological to condensed matter materials. It allows determining the structure of metal centres in proteins at subatomic resolution, where redox states can be distinguished, i.e. the effects of an individual electron with respect to the metal centre can be defined [11].

2. XANES FINGERPRINTS OF HEMOPROTEINS

Earlier reviews on XAS in biology and in the study of hemoproteins have been reported [12, 13]. XAS is especially powerful in elucidating the atomic structure around metal sites in biological compounds for the following reasons:

i) XAS is element specific. It probes the electronic transitions from an atomic core level towards delocalised electronic states in the continuum with selected symmetry. In a K or L_1 edge spectrum, s->p transitions from the 1s or 2s level of the metal to unoccupied states with p-symmetry are involved; in a $L_{2,3}$-edge spectrum, p->d and p->s transitions are involved, and so forth (see the Theory section). As the X-ray absorption edges from core levels of the atoms are well separated in energies, XAS probes the electronic state and the atomic structure around selected absorbing atoms in proteins, especially metal sites.

ii) The element of interest is never silent. Zn proteins and Cu^{+1} proteins, having filled 3d states, or antiferromagnetically coupled metal-ligand complexes, that are normally silent to UV/V or EPR spectroscopies, are accessible to XAS. XAS is sensitive to the redox state of the metal. As the effective positive charge of the metal increases, it becomes more difficult to extract an electron from the metal, and the absorption edge shifts to higher energies. The spin state of a transition metal can be recognised in several cases by looking at the features of a L-edge spectrum (probing directly p->d transitions, i.e. probing the unoccupied d-states of the metal); however also the pre-edge features of a K-edge spectrum probe unoccupied d-states, and the spin state of the metal, when p-d mixing occurs.

iii) It is a local structural probe. The EXAFS region, and, even more the XANES region, is extremely sensitive to the structural details of the metal site (coordination, overall symmetry, distances and bond angles), so that, in principle, an almost complete recovery of the geometrical structure within 5-6 Å from the absorbing site can be achieved from the experimental data. Experimentally, as shown in Fig. 1, the XANES spectra of various hemoprotein derivatives in solution differing for the 6^{th} iron ligand, i.e. myoglobins (Mb), hemoglobins (Hb) and cytochrome-C (CytC), show characteristic features for each ligand. These features are marker of the oxidation and spin state of the iron, and of the local Fe-heme-ligand structure. It is worthnoting here that on the basis of a comparison between hemin derivatives in SDS micelles, XANES and Resonance Raman spectra demonstrated that is possible to find a distal hydroxyl molecule instead of a proximal histidine imidazole as the 5^{th} iron ligand in five-coordinated high-spin ferric hemoproteins [14]. The rationale of any XANES study starts from the assumption that the spectra of two different Fe-heme proteins for which the iron has identical oxidation and spin state, and the same axial ligands should be very similar, with the same characteristic features, residual differences pertaining geometrical distortions. XAS can be really powerful in distinguish the environment of different metals in a protein. On the other hand, the XAS signal from multiple sites of the same metal contains the averaged sum of the signals from each site.

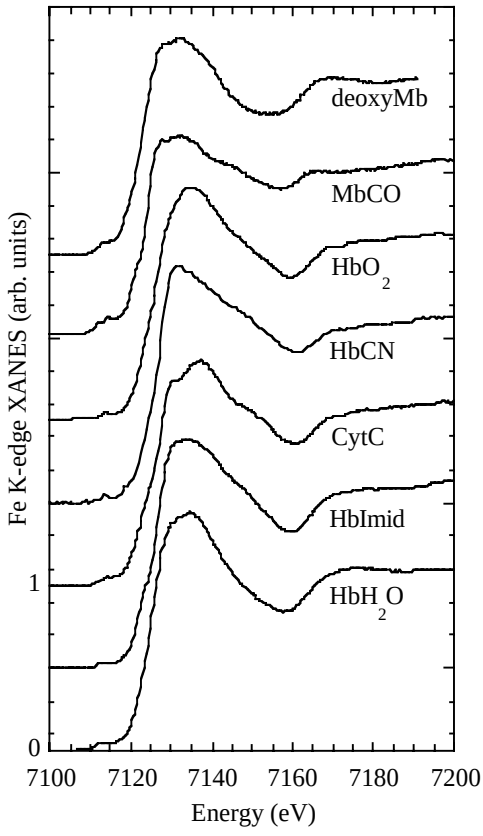

Fig. 1 - Fe K-edge XANES spectra of the hemoprotein derivatives in solution Sample sources: Hemoglobin (Hb) derivatives from human HbA; cytochrome-c (Cyt-c) from horse heart muscle; myoglobin (Mb) from sperm whale. From top to bottom (HS and LS indicate the spin state): HS Mb(II)deoxy; LS Mb(II)CO, LS Hb(II) O_2; LS Hb(III)CN; LS CytC(III) (having a metionine sulfur as sixth ligand); LS Hb(III)Imidazole; HS Mb(III) H_2O. Spectra taken at D21 beam line station of the LURE, and BM8-GILDA beam line station of the ESRF synchritrin facilities.

iv) It is suitable in any physical state of the sample. Crystals, powders, as well as solution samples can be studied, at any environmental conditions (pH, temperature, solvent, pressure) allowing either the comparison with already known X-ray structures at high resolution or to get information on protein that have proven difficult to crystallise **[11]**.

v) XAS spectra at the edge have no direct temperature dependence. It is well known (see the theory section) that nuclear vibrations induce exponential damping terms in the energy (or electron wavenumber k) scale of a XAS spectrum, i.e. Debye-Waller-like factors. In facts the XAS signal can be written as the sum of many terms identifying absorber-scatterer distances, or multiple scattering (MS) pathways (see the Theory section). Each term contains a sine function with an associated Debye-Waller damping factor $\exp(-2k^2\sigma^2)$, where σ is the root mean square deviation of the total MS length. This is the dominant term, which in the low energy part of the spectrum (for small k values), i.e. in the XANES region, is almost temperature independent and equal to one. As a consequence, XANES temperature dependent spectra (from the edge up to about 50 eV) can be structurally interpreted without taking into account nuclear vibration effects.

For all of these reasons, XAS can be applied to study both the structure and the dynamical behaviour of metallo-proteins, in particular hemeproteins. By changing the environmental conditions, different Fe-heme conformations can be explored if their conformational equilibria are opportunely modulated to obtain each of their different specific states. In Fig. 2, an example of the XANES ability to solve main average states of the Fe-heme aquomet-myoglobin is shown. XANES spectra of ferric aquomet-myoglobin from horse heart were acquired [15] as a function of pH between 5.3 and 11.3. At pH 11.3 temperature dependent spectra between T=90K and T=293K were collected as well. The experimental data solve three main conformations of the Fe-heme: the first (Fig 2a, dotted curve), at low pH, is related to high spin aquomet-myoglobin (Mb^+OH_2), the only derivative for which X-ray structures are reported [16-17]. The other two (Fig. 2b), at pH 11.3, are related to hydroxymet-myoglobin (Mb^+OH^-), and are in thermal equilibrium, corresponding to high spin Mb^+OH^- (dotted curve) and low spin Mb^+OH^- (solid curve). At this value of pH, the protein does not crystallise and no X-ray structure is available.

The temperature dependence of the XANES derivative spectrum of Mb^+OH^- (pH 11.3 at T=293K, 220K, 150K, and 100K) is shown in Fig. 2d. At least 6 isobestic points are discernible between T = 100K and T = 293K, giving the clearest experimental evidence for a two-state thermal equilibrium. The pH dependence of Mb^+ is depicted in Fig. 2c where XANES spectra at T=293K, pH= 5.3, 7, 8.7, and 11.3 are shown. Another spectral evolution is observed, with different (more undefined) isobestic points. It is clearly not possible to insert all the plotted spectra of Fig. 2 within the same isobestic points, hence they represent (at least) three structural states of the Fe-heme complex related to the multi-state equilibrium:

high spin Mb^+OH_2 <-> high spin Mb^+OH^- <-> low spin Mb^+OH^-

The term 'conformations' used here indicates main states reached by the Fe-heme depending on external conditions, so it is distinguished from 'substates' [18-20] indicating a multiplicity of protein states under the same environment. Either these main structural states selected under different conditions by XANES concide or not with substates, as it was suggested for MbCO [21], is a question to be solved by further experimental work. The structures of the three Fe-heme conformations were assigned according to multiple scattering simulations and fitting of the XANES data. According to a semi-quantitative approach, the chemical transition between Mb^+OH_2 and

high spin Mb^+OH^-, and the spin transition of Mb^+OH^-, are accompanied by changes of the Fe coordination sphere due to its movement toward the heme plane, coupled to an increase of the axial asymmetry.

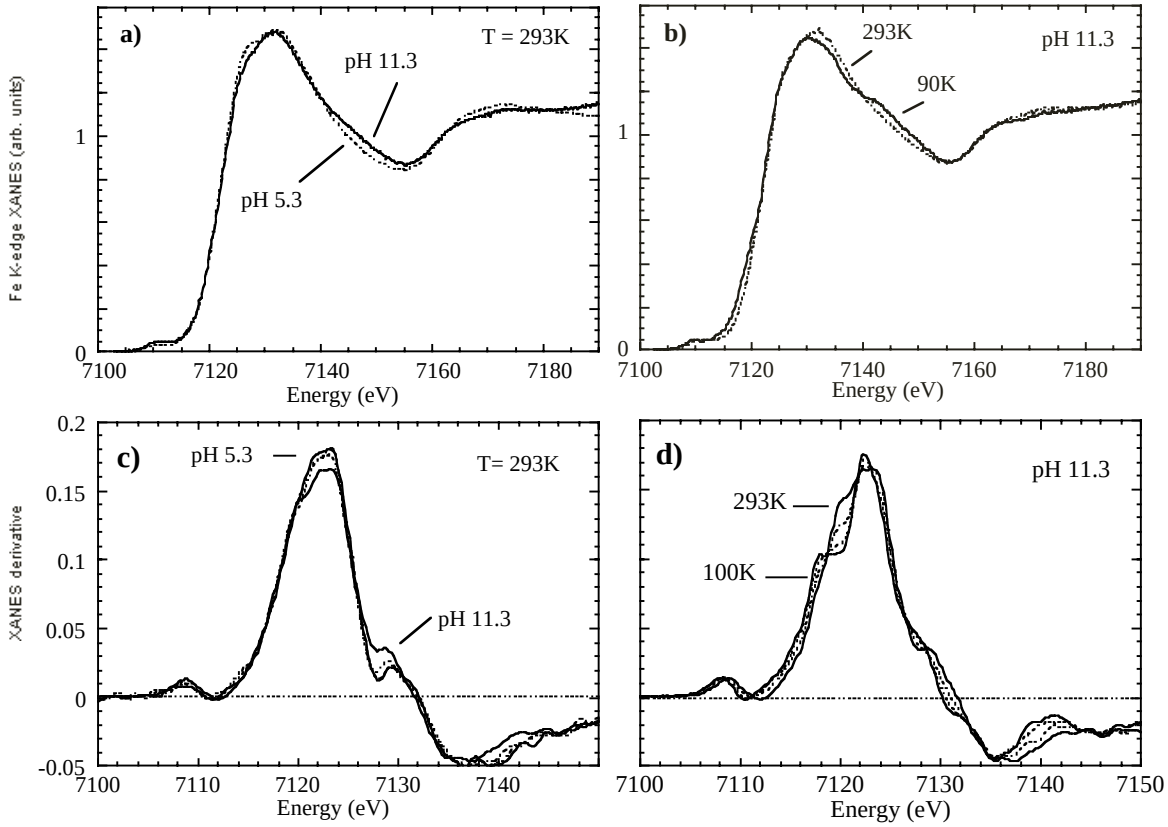

Fig. 2 Fe-heme conformations in aquomet-myoglobin as probed by XANES. **a)** Acid-alkaline transition at room temperature. Fe K-edge XANES spectra of Mb^+OH_2 (dotted curve), and HS Mb^+OH^- (solid curve). **b)** Thermal spin transition of alkaline Mb^+OH^-. Fe K-edge XANES spectra of HS Mb^+OH^- (dotted curve), and LS Mb^+OH^- (solid curve). **c)** Derivative spectra of the acid-alkaline transition at room temperature. **d)** Derivative spectra of the thermal spin transition of alkaline Mb^+OH^-; these latter spectra exhibit various isobestic points showing a perfect two-state transition without vibrational effects, i.e. the Debye-Waller terms are negligible in the 0-50 eV XANES range. Spectra are taken at D21 beam line station of the LURE synchrotron facility.

XANES can be applied to study high affinity (R) and low affinity (T) forms of hemoglobin [13]. Recently, XANES has been applied to study the cooperative homodimeric hemoglobin (HbI) of the mollusc *Scapharca inaequivalvis*. The Fe site structure in the recombinant wild-type and T72I mutant, the latter exhibiting enhanced oxygen affinity, and markedly reduced cooperativity [22] were investigated by measuring the Fe K-edge XANES spectra of their oxy, deoxy and carbonmonoxy derivatives, and the cryogenic photoproducts of the carbonmonoxy derivatives at T=12K [23]. The absorption edge of the XANES spectrum of the deoxy derivative of T72I HbI is blue-shifted with respect to the wild-type of about 1 eV. XANES spectra of the cryogenic photoproducts of the CO ligated wild-type (HbI*CO) and mutant (T72I HbI*CO) were acquired under continuous illumination at 12K. While in the case of HbI*CO the data indicate incomplete structural relaxation of the Fe-heme towards its deoxy-like (T) form, the relaxation in T72I HbI*CO is almost complete towards the proposed "high affinity" Fe-heme structure of T72I HbI. This evidence suggests that minor tertiary restraints affect the Fe-heme dynamics of T72I HbI,

corresponding to a reduction of the energy necessary for the T->R structural transition, which can contribute to the observed dramatic enhancement in oxygen affinity of this hemoprotein, and the decreased cooperativity.

These preliminary works showed that the relationships between protein function and the electronic and structural state of the Fe-heme start to be understood by XANES, allowing to connect, for the first time, a large body of experiments from different, unrelated techniques.

3. XANES THEORY: TOWARDS A QUANTITATIVE XANES ANALYSIS

A full quantitative analysis of the XANES spectra presents some difficulties mainly due to the theoretical approximation in the treatment of the potential [24,25] and the need for heavy time-consuming algorithms [26] to calculate the absorbing cross section in the framework of full multiple scattering approach [27]. For these reasons, the “XANES analysis” were considered a qualitative technique, used as a help for standard EXAFS studies [28] or more advanced investigations like the ones based on the analysis of contributions related to correlation functions of orders higher than two [29]. Few attempts were done to study the theoretical sensitivity of XANES to structural parameters and few examples of semi-quantitative comparison between experimental data and "ab-initio" calculations can be found in literature and almost related to known structural compounds [25].

Recently we have proposed a new method to perform a quantitative analysis of the low energy range [30]. A computational procedure, called MXAN, has been built up in the framework of the full multiple scattering (MS) approach in the XAS theory. A complete theoretical derivation of XAS is beyond the scope of this article; two recent exhaustive reviews on the actual state-of-the-art XAS theory can be found [31,32]. Here we give only some necessary details to understand the physical background.

3.1 - The absorption cross section. XAS concerns the study of the electronic transition from atomic inner shells to unoccupied states of the system under study. In this spectroscopy the absorption coefficient μ is measured as function of energy and its behavior is analyzed to extract both electronic and structural information. Typically the absorption coefficient decreases smoothly as the energy increases up to sharp discontinuities, the absorption edges, which are generated by photons with energy high enough to excite an electron from core levels. In Fig. 3 a pictorial view is shown of an absorption process by which a photon promotes an electron from the 1s core level of a metal atom in the molecular system to some possible unoccupied final electronic state in the continuum. The absorption coefficient μ is proportional to the density n_{ab} of the photoabsorber in the medium and can be written as $\mu(E) = n_{ab}\,\sigma(E)$, where $\sigma(E)$ is the total absorption cross section. This quantity exhibits strong oscillations with energy, the so-called X-ray Absorption Fine Structure (XAFS). The characteristic of XAS is that by tuning the X-ray energy it is possible to select the atomic species in which the excitation takes place and in this way the physical properties of the cluster surrounding the absorber can be explored by the photoelectron in its way out in the system. Because of the inelastic scattering of the photoelectron and the finite core-hole lifetime only a cluster of finite size is seen by the photoelectron making this spectroscopy a local probe around the absorber.

The high quality of the experimental data makes now possible several studies regarding the electron excitation dynamics and elucidates the interplay between geometrical and electronic structure in many systems from biological to condensed matter materials. Therefore a theoretical

scheme for interpreting such type of data is very important to give a guideline in the analysis. This scheme is provided by the multiple scattering theory that solves the problem to calculate the absorption cross section σ(E) in molecular clusters of any symmetry. The multiple scattering (MS) theory is essentially a method to calculate, from first principle, the electronic structure of polyatomic molecules and solids. This theoretical technique avoids many of the difficulties of the standard methods of quantum chemistry and band theory, leading to an accurate description of the wave function in molecules and solids of considerable stereo-chemical complexity. This method works in the real space without the need of any spatial symmetry and translation invariance. This last point is particularly important in the calculation of the X-ray absorption spectra from core levels because the presence of the core–hole in the final state breaks any translation symmetry. Using this theoretical approach one can calculate both the bound state and the continuum part of the molecular wave function.

The MS theory uses the so-called "muffin-tin" (MT) approximation for the shape of the potential of the cluster of atoms used in the calculation. This means that the space is partitioned into distinct atomic and interatomic regions. Each atom is enclosed in a sphere of specific radius, the so-called " muffin-tin " radius, and an "outer sphere" envelops the whole molecule. Three regions can be identified in this partitioning: atomic regions (spheres centered upon nuclei), extramolecular region (the space beyond the outer sphere radius), and an interstitial region of complicated geometry in which the molecular potential is approximated by a constant, position independent potential. As a further approximation the potential is spherically averaged within the atomic spheres and outside the outer region. A pictorial view of this type of potential is reported in Fig. 3

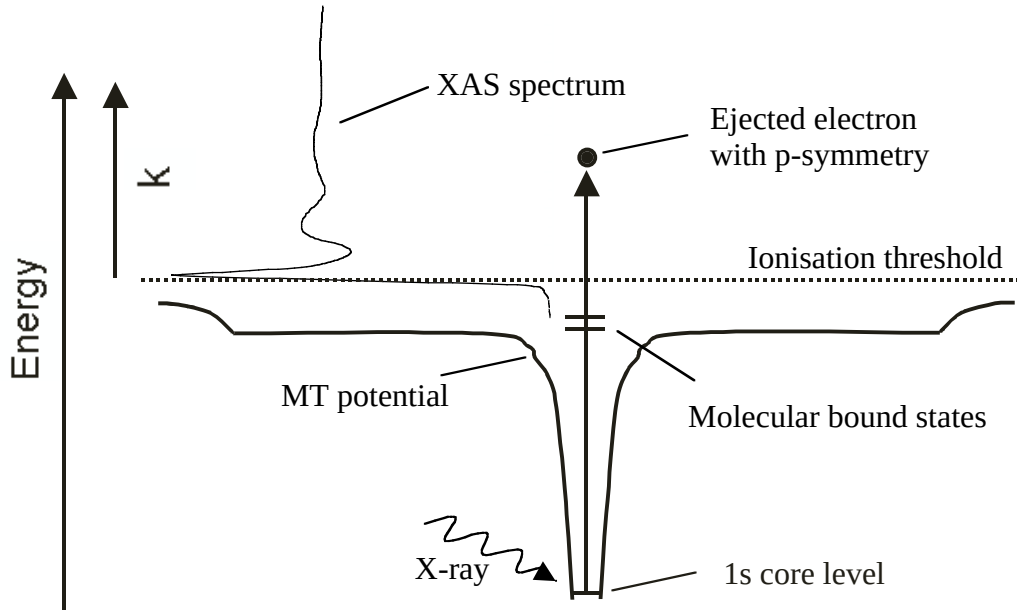

Fig. 3 Pictorial view of the Muffin Tin (MT) potential and the X-ray photo-absorption process.

Starting from the Fermi "golden rule" the photoelectron absorption cross section, within the dipole approximation, can be written as:

$$\sigma(\hbar\omega) = 4\pi^2 \hbar\omega\alpha \sum_f \left|\left\langle \phi_f \left| \vec{\varepsilon} \cdot \vec{r} \right| \phi_g \right\rangle\right|^2 \delta(\hbar\omega - E_f + E_g) \qquad \text{(Eq. 1)}$$

where $\hbar\omega$ is the photon energy, α=1/137 is the fine structure constant and the sum is over all the final states ϕ_f of energy E_f. The wave function ϕ_g is the ground state of energy E_g. The initial and final state wave functions are complicated many-body functions that can be written in terms of different electronic channels via the Slater determinants. It has been shown that it is possible to reduce this many-body problem of calculating the initial and final states of the system to a one-electron problem via a suitable complex optical potential. In this way the ground state is the core level of the absorbing atom while the final states ϕ_f can be calculated as the electronic state that describes a photoelectron scattered by the atoms in the system. To do this, it is necessary to solve the Schroedinger-like equation. Hereby atomic units are used in the mathematical expressions:

$$\left[\nabla^2 + k_f^2 - (V_{cou} + \Sigma(E))\right]\phi_f = 0 \qquad \text{(Eq. 2)}$$

where $k_f^2 = E = \hbar\omega - I_c$ is the photoelectron wave vector, $\hbar\omega$ is the photon energy and I_c is the ionisation energy. The term V_{cou} represents the Coulomb part of the total potential which contains electron-electron and electron-nucleus static interactions, and $\Sigma(E)$ is the so-called "self-energy" term, which is complex and energy dependent and represents the one-electron approximation of the non-local exchange and correlation potential [32]. The real part accounts for the energy dependence of the exchange interaction, while the imaginary part takes into account all the inelastic losses of the photoelectron in its way out in the system and it gives rise to the mean free path. The total potential $V = V_{cou} + \Sigma(E)$ constitutes a complex, 'optical' potential describing the interactions of the photoelectron moving in the molecule. Several approximations exist in the literature for this potential. It is well known for example that for metals one obtains very good agreement with the observed absorption spectra using a potential V where $\Sigma(E)$ is calculated on the basis of the real and energy independent X-α approximation [33], and convoluting the calculated spectrum with a lorentzian broadening function having an energy dependent $\Gamma_{tot}(E)$ width, which is related to the mean-free path λ_{tot} of the photoelectron by the relation [32]

$$\lambda_{tot} = \frac{1}{k}\frac{E}{\Gamma_{tot}(E)} \qquad \text{(Eq. 3)}$$

where $\Gamma_{tot}(E) = \Gamma_{mfp}(E) + \Gamma_c$. Γ_c is the core-hole lifetime and $\Gamma_{mfp}(E)$ is the energy dependent term accounting all the inelastic losses. A better approximation is provided by the Hedin-Lundqvist (H-L) potential [34,35] due to its energy dependent exchange and its imaginary part, which is able to reproduce rather accurately the observed mean-free path in metals [36].

To calculate the total cross section we need to know the explicit expression of the final state wave function inside the absorbing sphere due to the spatial localisation of the initial core level. At this stage it is convenient to re-write the total absorption cross section in terms of the imaginary part of the Green function $G(\vec{r}, \vec{r}'; E)$ of the system, which satisfies the equation

$$\left[\nabla^2 + k_f^2 - (V_{cou}(\vec{r}) + \Sigma(\vec{r}, E))\right]G(\vec{r}, \vec{r}'; E) = \delta(\vec{r} - \vec{r}') \qquad \text{(Eq. 4)}$$

The solution inside the atomic absorbing sphere can be derived using the MS theory. In this way, after the averaging over the polarisation of the light, the absorption cross section can be written as:

$$\sigma(\mathrm{E})=(\mathrm{l}_0+1)\sigma_0^{\mathrm{l}_0+1}(\mathrm{E})\chi^{\mathrm{l}_0+1}(\mathrm{E})+\mathrm{l}_0\sigma_0^{\mathrm{l}_0-1}(\mathrm{E})\chi^{\mathrm{l}_0-1}(\mathrm{E}) \qquad \text{(Eq. 5)}$$

for an initial ground state of angular momentum symmetry (l_0,m_0). The final angular momentum l is defined as $\mathrm{l}=\mathrm{l}_0\pm1$ according to the dipole selection rules. The quantity $\sigma_0^{\mathrm{l}}(E)$ indicates the atomic cross section of the absorbing atom at a given edge that is defined as:

$$\sigma_0^{\mathrm{l}}(E)=\frac{8\pi^2}{3}\alpha k(E+I_0)\sin^2\delta_{\mathrm{l}}^0\int_0^\infty r^3R_{\mathrm{l}}(r)\phi_{\mathrm{l}_0}(r)\,dr \qquad \text{(Eq. 6)}$$

and $\chi^{\mathrm{l}}(E)$:

$$\chi^{\mathrm{l}}(E)=\frac{1}{(2\mathrm{l}+1)\sin^2\delta_{\mathrm{l}}^0}\sum_m \mathrm{Im}[(I+T_aG)^{-1}T_a]_{\mathrm{l}m\mathrm{l}m}^{00} \qquad \text{(Eq. 7)}$$

is a structure factor carrying out all the information about the atomic cluster around the absorber. The quantity $\tau=(\mathrm{I}+\mathrm{T_aG})^{-1}\mathrm{T_a}$ is called scattering path operator, and it is a matrix whose dimension are given by $N_a(l_{\max}+1)^2$ where $\mathrm{N_a}$ is the number of atoms in the cluster and $l_{\max}$ is the maximum l-value in the spherical harmonics expansion of the T and G operators. The matrix $\mathrm{T_a}$ is a diagonal matrix defined through the atomic t-matrix t_{l}^i of the atom located at site i as $T_a=\delta_{ij}\delta_{LL'}t_{\mathrm{l}}^i$ with

$$t_{\mathrm{l}}^i=\frac{1}{\mathrm{k}}\sin\delta_{\mathrm{l}}\mathrm{e}^{\mathrm{i}\delta_{\mathrm{l}}} \qquad \text{(Eq. 8)}$$

where δ_{l} is the l-phase shift of the *i*-th atom that represent the phase difference between the incoming and outcoming partial l wave in the scattering processes [37]. The quantity G is the

amplitude of the free propagation between sites i and j [32]. Notice that in the case of isolated atom, i.e. if G=0, this structure factor is equal to one and the total cross section reduces to the atomic one. The atomic cross section is essentially without structures (in a one-electron approximation) and almost independent from the energy.

3.2 - The multiple scattering series expansion. To enlighten the physical meaning of the photoabsorption process, it is convenient to perform the matrix inversion in Eq. 7 by series:

$$(\mathrm{I}+\mathrm{T_aG})^{-1}=\sum_{\mathrm{n}=0}(-1)^{\mathrm{n}}(\mathrm{T_aG})^{\mathrm{n}} \qquad \text{(Eq. 9)}$$

provided that the spectral radius $\rho(\mathrm{T_aG})$ (maximum modulus of the eigenvalues) of the matrix $\mathrm{T_aG}$ is less than one. In such a case the structural factor $\chi^{\mathrm{l}}(E)$ becomes:

$$\chi^{l}(E) = 1 + \sum_{n=2} \chi_n^{l}(E) \qquad \text{(Eq. 10)}$$

with

$$\chi_n^{l}(E) = \frac{(-1)^n}{(2l+1)\sin^2\delta_l^0} \sum_m \mathrm{Im}[(T_a G)^n T_a]_{lmlm}^{00} \qquad \text{(Eq. 11)}$$

and $\chi_0^{l}(E) = 1$, $\chi_1^{l}(E) = 0$, since G is off-diagonal in the site indices.
Each term of the series has an expression increasingly complex with the expansion order, that can be conveniently expressed in the k space as

$$\chi_n^{l}(k) = \sum_{P_n} A_n^{l}(k, \vec{r}) \sin(kR^{TOT} + 2\delta_l^0 + \Phi_n^{l}(k, \vec{r})) \qquad \text{(Eq. 12)}$$

where the sum runs over all the P_n paths of order n starting from and ending at the central photoabsorbing atom with n-1 intermediate steps on the neighboring atoms, R^{TOT} is the corresponding total path length, and $A_n^{l}(k, \vec{r})$ and $\Phi_n^{l}(k, \vec{r})$ are the total amplitude and phase functions associated to the path P_n. Clearly $\chi_n^{l}(k)$ represents the partial contribution of order n to the photoabsorption coefficient of the cluster under study, coming from all process where the photoelectron emanating from the absorbing site o is scattered n-1 times by the surrounding atoms before escaping to free space after returning to site o. Due to the localisation of the initial core state only closed paths beginning and ending to the absorbing atom are possible. It is this peculiarity that entails the site specificity of the XAS spectroscopy and makes it a unique tool for studying structural problems and for probing higher order correlation functions in condensed matter. The development in Eq. 10 is the MS expansion with spherical wave propagators; the $\chi_2^{l}(k)$ term is the EXAFS signal. The simplest expression obtained by grouping the surrounding atoms in coordination shells is given [12];

$$\chi_2^{l}(k) = \sum_j \frac{N_j \, | f_j^{l}(\pi, k, R_j) |}{kR_j^2} e^{-2\sigma_j^2 k^2} \sin(2kR_j + 2\delta_l^0 + \Phi_2^{l}(k, R_j)) \qquad \text{(Eq. 13)}$$

where N_j is the number of equivalent backscattering atoms at a distance R_j from the aborbing atom, $f_j^{l}(\pi, k, R_j)$ is the backscattering amplitude, which is a function of both the atomic number of the backscattering atom and the length of the bond; the exponential term represent the Debye-Waller factor and can be derived considering the thermal vibration of the atoms in the harmonic approximation, σ_j^2 being the root-mean-square deviation of distance R_j from its equilibrium value. The loss of photoelectrons due to inelastic scattering processes can be accounted for in this formula by including a term $\exp(-2R_j/\lambda)$ where λ is the mean free path of the electron.
In Fig. 4, the backscattering amplitude $f_j^{l}(\pi, k, R_j)$ for $l=1$ (K-edges) and R_j=4.0 Å is plotted as a function of k for a transition metal atom (copper in this case) and for a light atom (oxygen) [38]. The comparison shows a complementary feature of the XANES and EXAFS techniques: XANES, contrary to EXAFS, is very efficient in probing a long distance between the absorbing metal and a light atom, but is rather insensitive to detect long metal-metal distances.

The interpretation of the XAS spectrum in terms of MS pathways of the photoelectron in the final state is meaningful only if there is numerical equivalence between the two sides of Eq. 9. This implies that the expansion on the r.h.s. must converge to the l.h.s. relative to some convergence criterion. From the matrix theory the absolute convergence is ensured if the spectral radius $\rho(T_a G) < 1$.

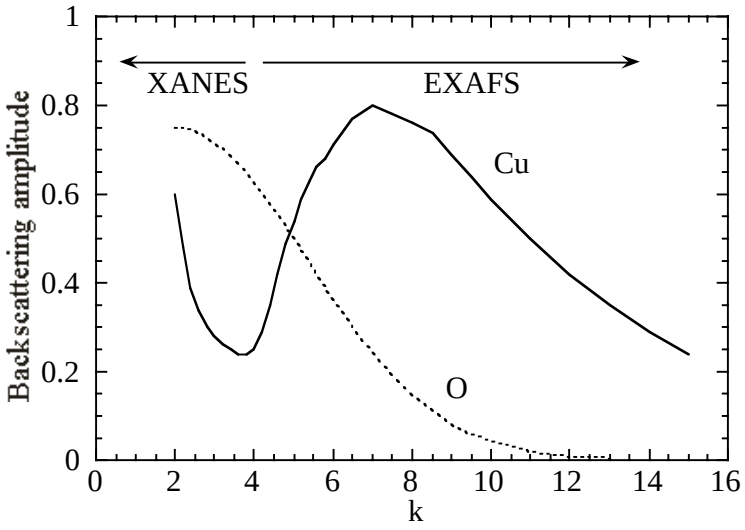

Fig. 4 - Backscattering amplitude function (in Å) versus k (in $Å^{-1}$) for copper and oxygen at R = 4 Å

This criterion is extremely useful since the absolute convergence entails the property that terms of order n in the series higher than a certain n_0 do not contribute appreciably to the sum. Now $\rho(T_a G)$ is a continuous function of the photoelectron wave number k, which goes to zero as k goes to infinity (since $t_l^i \to 0$ in this case) and tends to the infinity as k goes to zero because G is singular at k=0 due to the presence of the Hankel function in the definition of the propagators. As a consequence it must cross at least once the value ρ=1; the nearer to 1 is its value the slower is the convergence of the series.

According to the size of the spectral radius $\rho(T_a G)$, one can roughly divide the photoabsorption spectrum into different energy regions. Normally at low energy a great and/or infinite number of paths contribute to the shape of the spectrum, giving rise to the so-called XANES energy region. This is followed by the EXAFS energy region where only either a limited number of paths of low order or only paths of order n=2 contribute to the shape of the spectrum.

The general picture of a XAS spectrum that emerges from the preceding discussion is one in which oscillating signals with variable amplitudes are superimposed on a background of a more or less smooth atomic absorption. This picture is inspiring all the modern methods of analysis of the experimental XAS data.

3.3 - The MXAN method. Recently a new method to perform a quantitative analysis of the low energy range, the so called XANES energy region, i.e. from the edge up to 200 eV, has been proposed and applied to several systems [30]. This method, called MXAN, is based on the comparison between experimental data and many theoretical calculations performed by varying selected structural parameters starting from a putative structure, i.e. from a well defined initial geometrical configuration around the absorber. The calculation of XANES spectra related to the hundreds of different geometrical configurations needed to obtain the best fit of the experimental data is done in the framework of the full MS calculation, i.e. the scattering path operator τ is

calculated exactly, and the optimization in the space of parameters is achieved by the minimization of the χ^2 function in the parameter space with the MINUIT routines of the CERN library [39]. In this way the low energy part of the XAS spectrum is now fully available for a quantitative analysis and we can benefit for the extremely sensitive to the structural details of the absorbing site (overall symmetry, distances and bond angles) of this energy region. This is important in the study of many systems like extra-dilute systems, trace element analysis, local investigation of materials under extreme conditions and much more in biological systems where the low S/N ratio and the weak scattering power of the light elements limits the k-range of the available experimental data and the EXAFS can be barely exploited.

This new method needs of a phenomenological treatment of the inelastic losses to avoid the over damping at low energies produced by the complex part of the HL potential in the case of covalent molecular systems. It takes into account all the inelastic processes by a convolution with a broadening lorentzian function having an energy dependent width of the form $\Gamma(E) = \Gamma_c + \Gamma_{mfp}(E)$. The constant part Γ_c includes the core hole lifetime and the experimental resolution, while the energy dependent term represents all the intrinsic and extrinsic inelastic processes. The $\Gamma_{mfp}(E)$ function is zero below an onset energy E_s (which in extended systems corresponds to the plasmon excitation energy) and begins to increase from a value A_s following the universal functional form of the mean free path in solids. Both the onset energy E_s and the jump A_s are introduced in the $\Gamma_{mfp}(E)$ function via an arctangent functional form to avoid discontinuities. Both numbers are derived on the basis of Monte Carlo search at each step of computation.

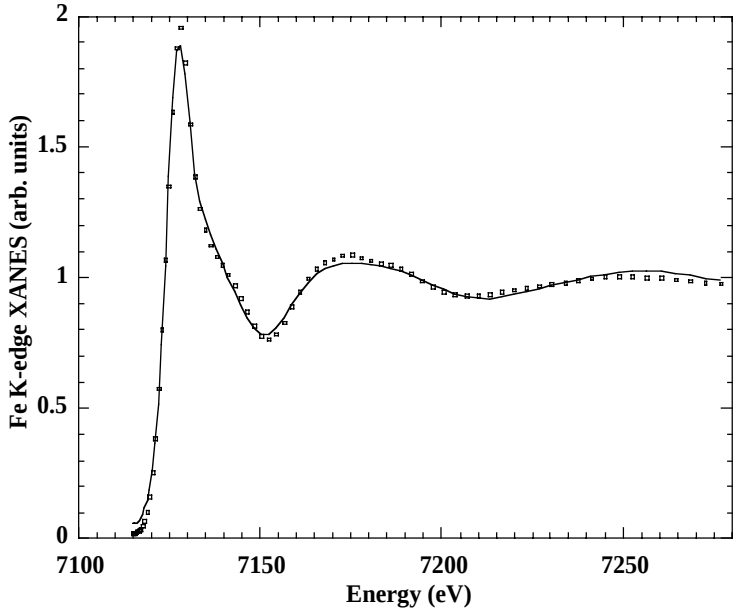

Fig. 5 MXAN analysis of Ni^{2+} aqueous solution. Circles: experiment. Solid curve: theoretical best fit.Starting from a distorted, orthorhombic $Ni(H_2O)_6$ cluster, The best fitting structure has octahedral symmetry and an oxygen-metal distance of 2.03±0.03 Å Hydrogen atoms are included in the calculations.

This type of approach is justified on the basis of a multi-channel multiple scattering theory that is the generalization of the standard MS approach to account all the possible electronic channels that enter in the many-body expansion of the wavefunctions. In the ‘sudden’ limit [40], the net absorption is given by a sum over all the possible channels that represent each of the final states allowed in the photo-absorption process. They include the fully relaxed configuration, which gives

the main contribution to the spectrum, and all the other possible excited states of the (N-1)-electron system. By assuming that the channels coming from the excitation of the N-1 electrons are very near in energy, the total absorption is given by a convolution of the one-particle spectrum calculated with the full-relaxed potential with a spectral function representing the weight of the other excited states. Hence the total XAS cross section can be written as

$$\mu = \sum_n \mu_n \xrightarrow[\Delta E \to 0]{} \int \mu(\omega - \omega') A(\omega') d\omega' \qquad \text{(Eq. 14)}$$

The assumption is made that the spectral function A(ω) is well approximated by a Loretzian function with the energy dependent width Γ(E) previously defined. Obviously, in the cases when contributions from one or more of these excited states become relevant, they must be considered explicitly in the calculation. As test cases of the new method, the analysis of the K-edges of Ni^{2+}, Fe^{2+}, Co^{2+}, and Cu^{2+} ions in aqueous solution has been carried out [30,41,42].

The theory.vs.experiment fit in the case of nichel is reported in Fig. 5. This ion is often used as test case due to the well-defined formal valency of the ionic species and the very simple geometry around the absorber. The solid line corresponds to a calculation related to the best-fit structure that is geometry with an octahedral symmetry and an oxygen-metal distance of 2.03±0.03 Å. Hydrogen atoms are included in the calculations. The agreement between the experimental data and the best-fit theoretical curve is good in the whole energy range; small discrepancies remain in the intensity of the resonance at 15 eV essentially due to the muffin-tin approximation for the shape of the potential.

We emphasize that the multiple scattering theory is a very general approach to calculate physical quantities from “first principles”; to this respect its field of applications is not limited to the XAS spectroscopy but many other kinds of experiments can benefit of this theoretical approach to have a solid background for the physical interpretation [43].

4. MXAN ANALYSIS OF MbCO AND Mb*CO IN SINGLE CRYSTAL

XANES can be applied to study protein metal sites both in crystals and solution. The $P2_1$ single crystal of sperm whale myoglobin is a powerful laboratory system for XANES studies of myoglobin. The XANES spectrum of sperm whale myoglobin in solution can be ‘experimentally’ decomposed into two almost perfectly polarised spectra by collecting measurements from the single crystal formed by this protein [44]. A pictorial view of the crystal unit cell, including the Fe-heme sites of the two symmetry related myoglobin molecules, is represented in Fig. 6a. The monoclinic unit cell is seen along a projection parallel to the b-axis. It is possible to rotate the crystal to have the X-ray polarisation vector ε oriented parallel either to the a* axis of the crystal, which forms an angle of 23° with the heme normal, or parallel to the c axis that forms an angle of 86° with the heme normal, i.e. is almost parallel to the heme planes. As a consequence, the ε // c spectrum contains 99.5% contribution from scattering pathways within the heme plane, and the ε // a* contains 15% contribution from scattering pathways within the heme plane and 85% contribution from scattering pathways along the heme axis. The solution spectrum, and the ε // c and ε // a* polarised spectra of the carbonmonoxy-myoglobin (MbCO) single crystal are reported in Fig. 6b.

The photolysis of MbCO at low temperature, i.e. the dissociation of the CO molecule from the Fe-heme complex in the hydrophobic core of myoglobin (Mb), induced by visible light, is a paradigmatic event of protein dynamics [45] that has been addressed by many theoretical and experimental studies [4, 46-50]. This process is represented in a simplified scheme by the three-well model: MbCO <--> Mb*CO <--> Mb; in which MbCO is the starting main state of the protein, Mb the final main state when the CO molecule is in the solvent, and Mb*CO represent all the intermediate states when the CO molecule is in the protein matrix.

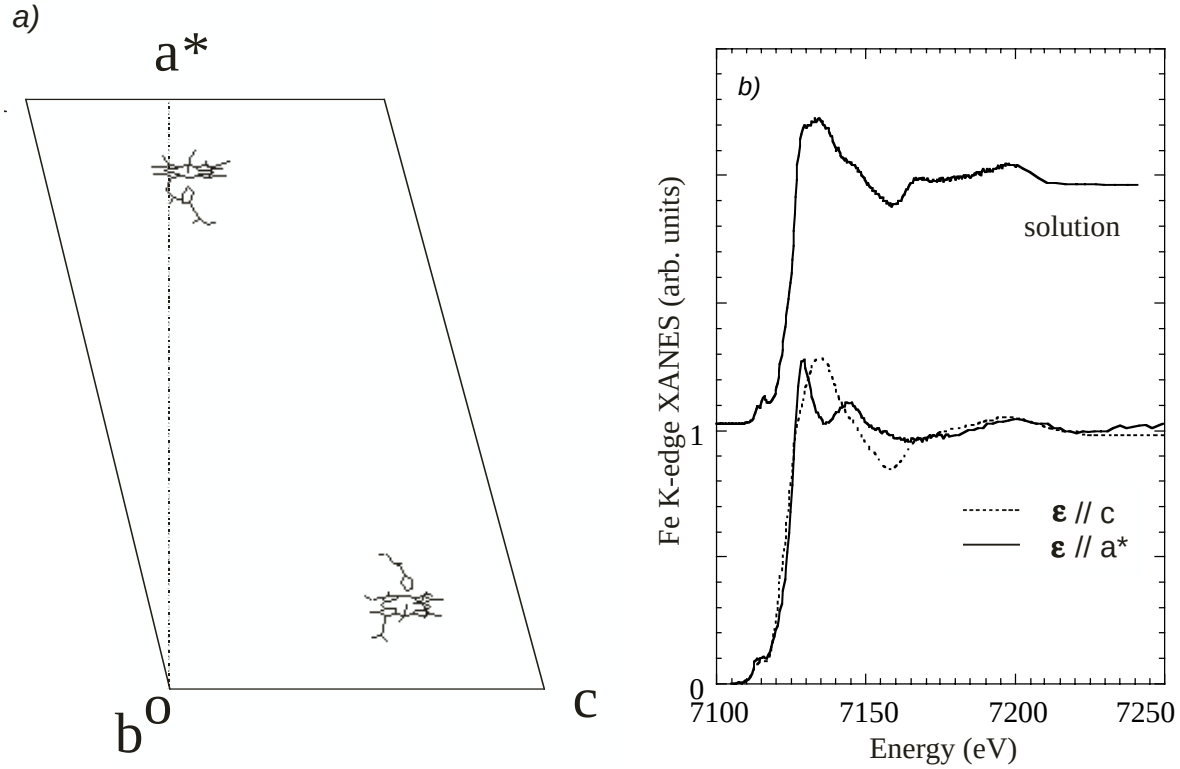

Fig. 6 a) Pictorial view of the sperm whale myoglobin $P2_1$ crystal unit cell with the Fe-heme sites of the two symmetry related myoglobin molecules. b) Fe K-edge XANES spectra of sperm whale MbCO in solution (upper curve); polarised XANES spectra from MbCO single crystal (lower curves). Spectra are taken at BM8-GILDA (solution) and BM32-IF (crystal) beam line stations of the ESRF synchrotron facility.

The X-ray crystal structures of MbCO and Mb at a resolution of 1.15 Å [51,52] show that concerted motions of the iron, the heme, and helices E and F of the protein accompany the CO dissociation at room temperature. At room temperature the photodissociated CO molecule rebinds to the iron in the microsecond time scale. At T < 30K the CO rebinds very slowly [53] so that almost 100% conversion to the photoproduct can be achieved in the experimental time window of standard techniques, but the protein matrix remains frozen in the conformation of ligated MbCO.

X-Ray diffraction studies of the cryogenic Mb*CO photoproduct at T=20K [46] and T=40K **[4]** reported different positions of the CO molecule in the heme pocket. It has been proposed [48] that the different positions found correspond to migration of the CO molecule. In the recent years, the availability of both X-ray dynamic focusing elements and high energy resolving array fluorescence detectors, has allowed to collect polarised XANES spectra of a small single crystal (0.2*0.2*0.3 mm^3) of MbCO and its photoproduct Mb*CO at 20K, obtained under continuous illumination by a white light source. In these experimental conditions, a single photolised species has been observed by X-ray diffraction, with the CO molecule located in a ‘primary’ docking site above pyrrol C of the heme, at a distance of about 2.8-3.6 Å from the iron [46,48]. Details on the polarised XANES experiment have been previously reported [54].

The XANES experimental results are shown in Fig. 7. In the ε // a* polarisation, nearly parallel to the Fe-C bond, the photolysis has dramatic effects on the spectrum: a completely new spectrum appears with different values of edge position, and prominent features. In the ε // c polarisation, more subtle changes can be found, i.e. a red-shift of the maxima at about 7200 and7270 eV in Mb*CO relative to MbCO, suggesting a change in the frequency of the main oscillating component of signal, in agreement with the partial elongation of the distance between iron and the nitrogen belonging to the pyrrolic ring reported by X-ray diffraction and by previous EXAFS data in solution [55].

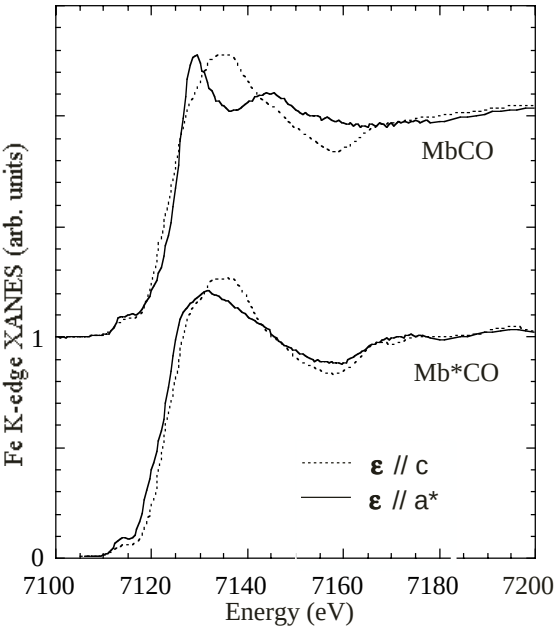

Fig. 7 Polarised fluorescence XANES spectra of a MbCO single crystal were acquired at T=100K in a helium atmosphere, by rotating the crystal mounted in a quartz capillar around the **b**-axis, i.e. by changing the X-ray polarisation vector **ε** from the **ε** // **c** to the **ε** // **a*** orientation. Then the crystal was cooled at T = 20K, and the Fe-CO photolysis was achieved using white light (500-600 nm) from a fibre optic illuminator lasting about three hours, with a photolysis rate of about 0.01 s^{-1} for an integrated power density of illumination of 0.05 mW mm^{-2}. Upper curves: MbCO at T<100K. Lower curves: Mb*CO at T=20K.

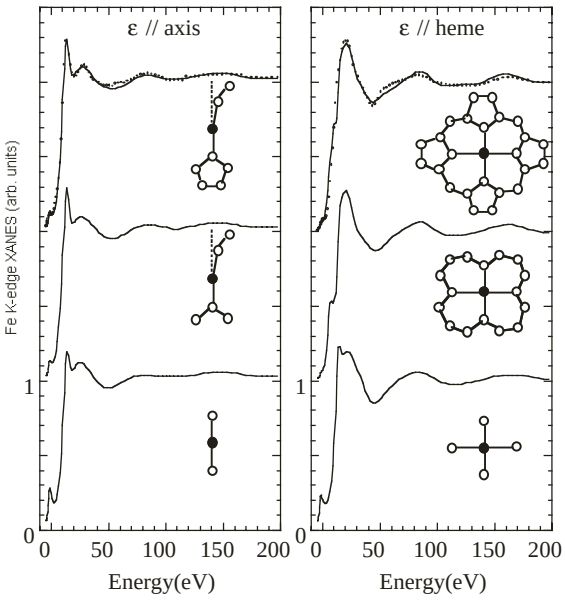

Fig. 8 MXAN analysis of the polarised XANES data of MbCO. Upper curves: best fit results; circles: experiment. solid curve: theoretical best fit. The effect of the cluster size to the XANES features is shown by the lower curves, related to the 1-shell calculation (bottom) and 2-shell calculation (centre). Experimental data cannot be explained by a 1-shell analysis. The structural results for the selected parameters are discussed in the text.

The experimental data have been analysed with the MXAN fitting procedure [56]. An important parameter for any XANES simulation is the size of the atomic cluster that determines the experimental features. It depends on the electron mean free path and the core-hole life time and can

change relevantly depending on the structural symmetry and thermal disorder. In the case of myoglobin, a cluster of 32 atoms, i.e. the porphyrin macrocycle, the histidine imidazole, and the CO molecule accounts for all the experimental features. In Fig. 8, the effect of the cluster size on the XANES calculations of MbCO is shown, together with the MXAN fit of the polarised components of the experiment.

The molecular potential for the nearest atoms, i.e. the FeN_5CO cluster, has been obtained by self-consistent field (SCF) method imposing the formal valence of each atom [57,58]. Muffin-tin radii have been chosen on the basis of the Norman criterion, and the exchange correlation part of the potential has been determined by the X-α approximation. Inelastic losses have been included using the method described in the Theory section (Eq. 14). Starting from a chosen configuration of the absorbing site, the MXAN procedure reached the best-fit conditions in reasonable time by the minimisation of χ^2 in the space of n selected structural parameters: the first shell distances d(Fe-N_p), d(Fe-C), d(Fe- N_{his}), where N_p indicates the pyrrolic nitrogens of the porphyrin, N_{his} indicates the imidazole nitrogen of the histidine; the tilting angle α between the Fe-C vector and the heme normal, the bending angle β between the Fe-C vector and the C-O bond, and the C-O bond length. During the fit, the imidazole ring of the histidine, and the pyrrolic rings of the porphyrin rigidly follow the motion of the N_{his} and N_p atoms, respectively.

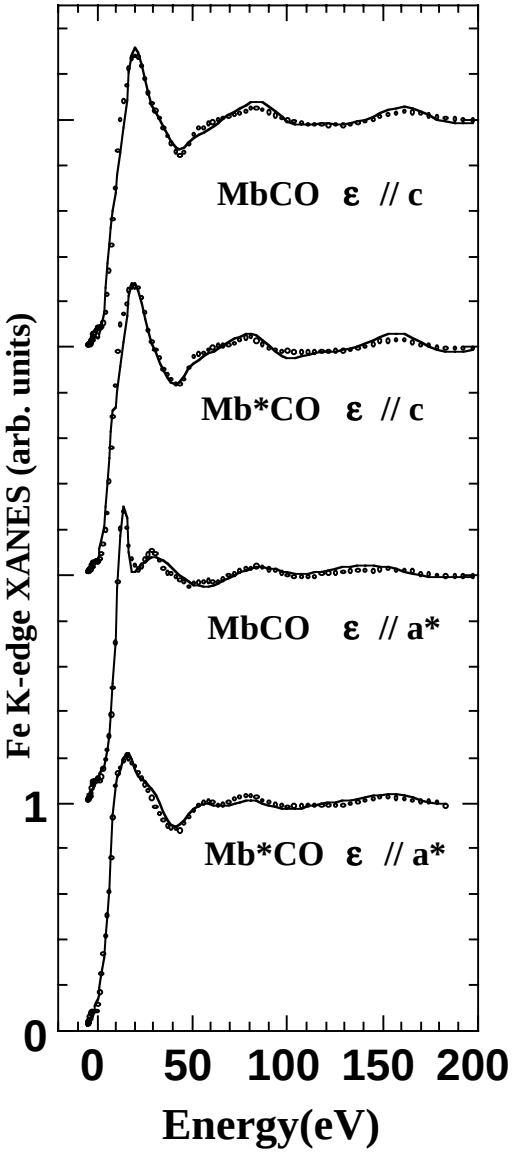

Fig. 9 MXAN best fits (solid lines) for the polarised spectra of MbCO and Mb*CO.(circles). The **ε // c** spectra are used to fit the Fe-N_p distance, while the **ε // a*** spectra are used to fit all the other n-1 parameters. A constant experimental error corresponding to a noise to signal ratio of 0.01 was chosen for all the spectra normalised at the edge jump. The value of χ^2/n found at the best-fit conditions were 3.46, 3.08, 2.09 and 1.85 respectively for MbCO **ε // c**, Mb*CO **ε // c**, MbCO **ε // a***, and Mb*CO **ε // a***. Alignment of the theoretical and experimental spectra has been obtained with an energy shift of 7115.5 ± 0.3 eV. A value of Γ_c = 2.7 ± 0.1 eV results from the fit procedure, in good agreement with the sum of the known value of core-hole lifetime (1.2 eV) and experimental resolution, which is about 1.4 eV. This high value is due to the experimental conditions, the crystal being placed in a glass capillary and embedded in helium atmosphere during the data acquisition runs. The plasmon-like excitation included in the fit has an onset at 15 ± 4 eV and amplitude of 10 ± 3 eV.

In Fig. 9 the best fit (solid curves) of the experimental XANES spectra of Fig. 7 are shown, after optimisation in terms of the structural parameters. The experimental data are plotted in circles. First of all, it is noticeable that the calculations at the best-fit condition are able to reproduce the dramatic difference between MbCO and Mb*CO in the ε // a* spectra, consequent to the change in the coordination symmetry.

The fits are highly sensitive to the first neighbour distances, to the bending angle β, and to the C-O bond length. The Fe displacement from the heme plane, the tilting angle α of the Fe-C vector, and the tilting angle of the histidine residue have been also considered in preliminary runs, but the fit came out poorly sensitive to them. The XANES sensitivity to the tilting angle α is intrinsically low for solution spectra, but can be stronger in polarised spectra, as the intensity of the XANES signals from electron pathways including the Fe-C vector vary approximately as $\cos^2(\alpha')$, α' being the angle between **ε** and this vector. In the case of the **ε** // a* spectra of MbCO, $\alpha' \approx \alpha$, and according to the more recent X-ray structures, $\alpha = (6 \pm 3)°$. Around this low value of α, variations of the $\cos^2(\alpha)$ function, and in turn the XANES sensitivity to α, is very small.

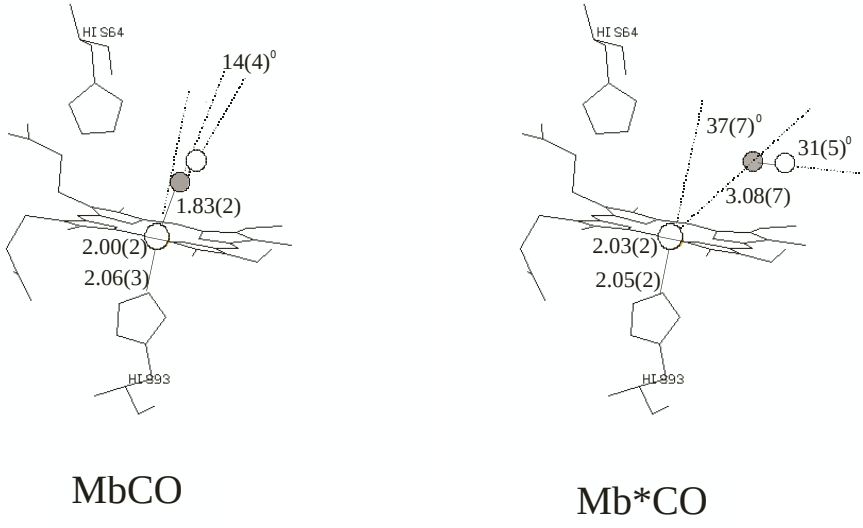

Fig. 10 MXAN best fit results for MbCO and Mb*CO. The values found for the d(Fe-Np), d(Fe-Nhis), d(Fe-C), and the tilting and bending angle of the CO are indicated. Number in parenthesis are the statistical errors on the last digit as evaluated after the optimisation by the MIGRAD algorithm of the MINUIT package. Errors take into account all the parameter correlations (but not the non-linearities).

The structural results relative to MbCO and Mb*CO are summarised in Fig 10. A measure of all the relevant parameters of the Fe-heme-CO cluster, in particular the Fe-C-O bending angle in MbCO, has been obtained.

In Fig. 11, we show the comparisons between the experimental spectrums of MbCO, the calculation related to the MXAN best-fit structure, and other calculations related to different structural determinations of the heme site geometry obtained by X-ray diffraction. They include the low resolution data by Kuryian et al. [59] and two high-resolution X-ray structures [51,52] by Kachalova et al. at room temperature (PDB code 1BZR), and by Vojtechovsy et al. at T=100K (PDB code 1A6G). These latter two structures are essentially identical, apart from the CO binding geometry. Our geometrical determination is in complete agreement with the results of Vojtechovsy et al., considering that a resolution of 1.15 Å in a X-ray diffraction determination should correspond to an uncertainty in the atomic position of about 0.05 Å [60].

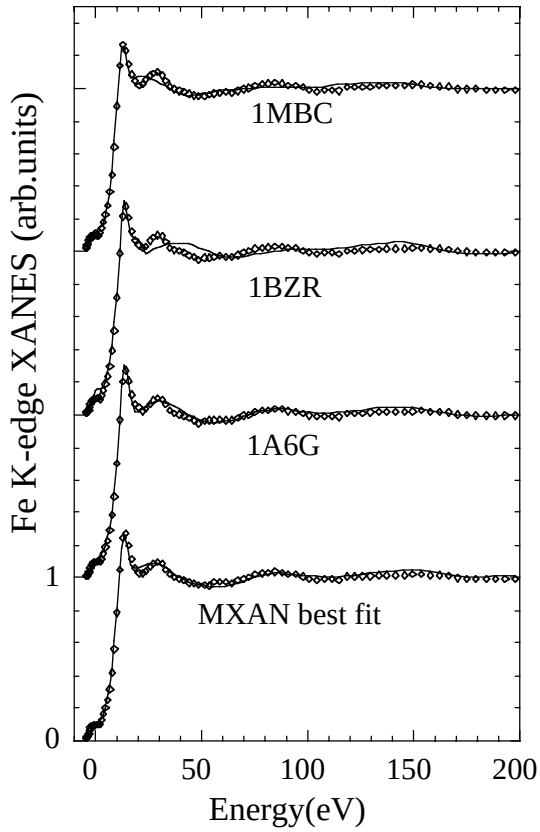

	Fe - Np	Fe - Nhis	Fe - C	α	β	C - O
1MBC 1.5Å	1.97	2.19	1.92	3	38	1.17
1BZR 1.1Å	1.98	2.06	1.73	4	7	1.12
1A6G 1.1Å	1.98	2.06	1.82	9	9	1.09
MXAN fit	2.00(2)	2.06(3)	1.83(2)	--	14(4)	1.07

Fig. 11 MbCO. Comparison between the ε // a* XANES spectrum (circles) and XANES calculations done (solid lines) using the structural determinations by the MXAN fit, and by X-ray diffraction. The PDB code and the resolution of each reported X-ray structure is indicated. Distance units in the table: angstrom. Angle units: degrees. The values in parenthesis are the statistical errors as evaluated by the fitting procedure.

The Mb*CO species has been analysed using the same set of structural parameters. In Fig. 12 we report the comparison between the experimental data of Mb*CO, the calculation related to the geometry at the best fit condition, and some of the more recently reported X-ray structures. Our results are in rather good agreement with the X-ray diffraction data [48] by Teng et al. (PDB code 1AJH), and differ more significantly from that [46] by Schlichting et al**.** (PDB code 1ABS). The MXAN fit is sensitive to the distances between the iron and pyrrolic nitrogens and the ligated imidazole nitrogen of histidine, but it is also highly sensitive to the distance and orientation of the far CO molecule, allowing a determination of the Fe-C distance with a statistical error of 0.07 Å and of the angles α and β with an error of 7° and 5° respectively. The fit of **ε** // a* Mb*CO is sensitive to the tilting angle α in this case because of its higher value.

Small changes in the structural geometry, essentially the CO position and orientation, even in the case of the unligated Mb*CO induce such relevant differences in the XANES calculation, giving access to structural details of the low temperature photoproduct of MbCO with high precision. The sensitivity to the position of the CO molecule is particularly high in the XANES region because the scattering power of light elements is large and comparable with that of heavy atoms in the EXAFS energy range (see Fig. 4). At higher energy, i.e. in the EXAFS region, the signal from light atoms decreases so much that it is hard to get more information than the first shell distances. The ability to perform a quantitative analysis of the XANES energy region allows determining some relevant structural parameters that are normally impossible to recover by the standard analysis of the EXAFS data. In the 1AJH and 1ABS structures of Mb*CO the CO molecule is located in a primary docking site, in the distal cavity. In Fig. 12, however, we have inserted also the 1DWT structure concerning the photo-relaxed (Mb**CO) horse myoglobin, in which the CO molecule is reported sitting in a

secondary docking site, in the proximal cavity. This secondary docking site can be populated at low temperature by illumination with an intense laser light [50].

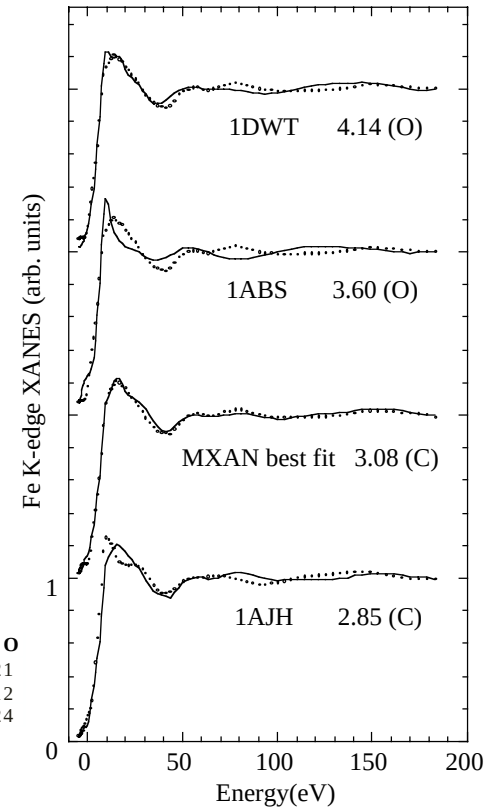

	Fe - Np	Fe - Nhis	Fe - C	α	β	C - O
1AJH 1.7Å	2.00	2.11	2.84	23	45	1.21
1ABS 1.5Å	1.97	2.25	3.60*	27*	54	1.12
MXAN fit	2.03(2)	2.05(2)	3.08(7)	37(7)	31(5)	1.24

Fig. 12 Mb*CO. Comparison between the ε // a* XANES spectrum (circles) and XANES calculations done (solid lines) using the structural determinations by the MXAN fit, and by X-ray diffraction. Distance units in the table: angstrom. Angle units: degrees. In the figure, also the simulation from the 1DWT is shown, pertaining the photo-relaxed structure (Mb**CO) reported for horse myoglobin [50]. In this structure, the CO occupies a secondary docking site in the proximal cavity. The distance from the iron to the CO molecule (i.e. the nearest between the C and O atoms) according to the authors is indicated.

According to our calculations, it seems possible to discern, by XANES of single $P2_1$ crystals, different intermediate states of the ligand binding processes in myoglobin i.e. different ligand docking sites, by using opportune experimental protocols including low temperature, laser pumping, mutants having smaller association rates [61], already applied for populating these states in diffraction studies.

4. MXAN ANALYSIS OF HEMOPROTEINS IN SOLUTION

The MXAN analysis can be used to extract the Fe-heme structure by hemoprotein in solution. It is expected the accuracy in the structural determination to be worse than in the case of the $P2_1$ single crystal, due to the convolution of the polarised contributions in the solution spectrum. Another difficulty concerns the use of the Γ(E) function: as seen in the Theory section, the use of a phenomenological function corresponds to introduce three non-structural parameters, namely Γ_c, E_s and A_s, in the fitting procedure. However, to take into account the strong asymmetry of the Fe-heme site, the function Γ (E) used to fit solution samples has a vectorial form with different values of the E_s and A_s parameters for the two polarised components of the solution spectrum. As total, five non structural parameters: Γ_c, E_s^{normal}, E_s^{heme}, A_s^{normal}, A_s^{heme} are used in the fitting procedure. Theoretically it is justified considering that all the physical quantities involved, in particular the dielectric function associated to the calculation of the self-energy of the system, must have the same

symmetry of the geometrical cluster. As a consequence the mean free path term is largely anysotropic; it turned out evident by looking at the systematic difference in the values E_s found for the ε // c and ε // a* polarised spectra.

In Fig. 13 the experimental XANES spectra (circles), and the theoretical best fits (solid lines) from the MXAN analysis of cyanomet-hemoglobin (HbCN), carbonmonoxy-myoglobin (MbCO) and oxy-hemoglobin, are compared. In the table of the figure, the values of the axial distances and of the bending angle β of the CN, CO, and O_2 ligands are shown. The spectra of these compounds are rather similar in the EXAFS limit, whereas are well distinguished in the XANES range. The intensity ratio C/D of the two main peaks C and D of the spectra decreases in the order CN -> CO -> O_2 and this feature was attributed in previous studies on myoglobin as a marker of the ligand bending angle β [44] that were evaluated as 0° in MbCN, 40° in MbCO and 70° in MbO_2 . the XANES

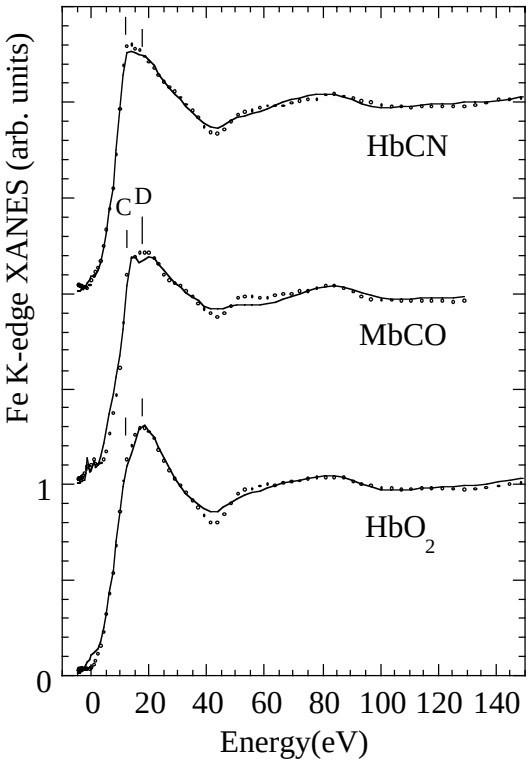

	χ^2/n	Fe - Nhis	Fe - L_1	β	L_1-L_2
HbO2.	2.44	2.18(4)	2.02(2)	65(12)	1.31
MbCO cryst	2.5	2.06(3)	1.83(2)	14(4)	1.07
MbCO solut	6.13	2.02(4)	1.72(4)	6(4)	1.11
HbCN	1.32	2.22(7)	2.03(5)	< 30	1.05

Fig. 13 *XANES experimental spectra (circles) of HbCN, MbCO and HbO_2 in solution. Sample sources: Hemoglobin (Hb) derivatives from human HbA; myoglobin (Mb) from sperm whale. Solid lines represent the theoretical calculations corresponding to the MXAN best fit. The structural results are reported in the table. Distance units: angstrom. Angle units: degrees. Spectra taken at D21 beam line station at LURE, and BM8-GILDA beam line station at ESRF.*

In particular for MbCO the bending angle reported was in agreement with the X-ray structure reported by Kuriyan et al. [58]. However according with the more recent investigations by XRD [51,52] infrared spectroscopy studies [62,63], and according with our recent MXAN analysis [56] the binding of CO to the Fe-heme in myoglobin is nearly linear, thus it seems that the interpretation of difference between CN, CO, and O_2 ligated myoglobin and hemoglobins has to be changed. Notwithstanding the intensity ratio C/D is theoretically very sensitive to the ligand bending angle Fe-L_1-L_2, other structural determinant (such as the Fe-His, the Fe-L_1, and the L_1-L_2 distances) can affect the shape and intensities of the same XANES features. In the table the results of a preliminary MXAN analysis (unpublished data) are presented. It is important to stress here that the XANES signal of human hemoglobin is as an average between the 2α and 2β subunits of the protein, while the present MXAN analysis includes a simple one-state model in the structural fit. Results should

be more reliable starting from a more realistic model, which accounts for the heterogeneity of the subunits, i.e. a two-state model. However according to these first results the difference in the intensity ratio C/D between HbCN and MbCO can be explained by a different axial ligand symmetry at the Fe site, HbCN exhibiting elongated 5^{th} and 6^{th} ligand distances than MbCO. On the other hand, HbO_2 has the same axial distances as HbCN, and the intensity ratio C/D change going from HbCN to HbO_2 should depend on the large difference in the bending angle and in having an elongated O-O bond with respect to the C-N bond. Further XANES differences should certainly be due to the change of the ligand atoms themselves, that influences the atomic t-matrix of Eq. 7 and in turn the structure factor of Eq. 6. Last, an interesting comparison between the MXAN analysis on MbCO in the crystal and in solution is reported. There is a difference in the Fe-C distance larger than the statistical errors between the two determinations. However, the χ^2/n value of the fit in solution is rather large, due to the systematic disagreement, which is observed between theoretical and experimental data in solution at 40-60 eV. This discrepancy probably reflects the poor approximation used for the broadening function $\Gamma_{mfp}(E)$ via an arctangent form.

5. CONCLUSIONS

The MXAN analysis represents only an encouraging step forward in the long way towards a full understanding of XANES. It can start to be applied in biology with care, calibrating the non-structural parameters of the theory on reliable model systems, and combining XANES with other related techniques, especially EXAFS. In the same time, as both structural and electronic information are present in the low energy region, it would be very important to have a more reliable XANES theory, avoiding the need of a phenomenological treatment of some aspect of it. Theoretical efforts [32] address the inclusion of vibrational effects in the high energy part of the XANES spectrum: the effects of atomic vibrations should be included in the theoretical simulations if the fitting procedure is extended beyond the near edge, since their damping effect interferes with the electronic damping due to the imaginary part of the optical potential. Other more difficult theoretical tasks include the elimination of the Muffin-Tin approximation, the implementation of a multi-channel multiple scattering theory, and the solution of the problem of the optical potential in the final state.

Notwithstanding all these limitations, as a matter of facts, even with the present approximations a structural analysis by full spectrum fitting seems possible for the systems considered here. In this work we have shown how the Fe K-edge XANES can be used on hemoproteins to probe redox changes and the spin state of the Fe-heme, due to the fingerprints properties of the pre-edge and the rising edge region. The ligand association-dissociation to the Fe-heme is a dramatic event as looked by the XANES probe; as the photolysis of the ligand-Fe bond in hemoproteins can be triggered by light, and some transient intermediate can be trapped at low temperature, thermodynamic aspects linked to the ligand rebinding barriers could be certainly studied. The local structure at a resolution comparable with that of the more recent X-ray diffraction data seems now available via the MXAN method, rendering possible a quantitative approach to ligand linked conformational changes and to the study of R-T forms, i.e. of cooperativity in hemoglobins. Data from crystals and solution can be easily compared and the effect of the crystal field on the Fe-heme could be investigated. MXAN investigations could include redox induced changes of the Fe-heme structure in electron transfer hemoproteins and the spin-structure relationships in hemoproteins in thermal spin equilibrium. In such a way, XANES spectroscopy starts to reveal its unique abilities in allowing an almost complete description, in a single experiment, of the electronic and structural determinants of ligand binding at the Fe-heme.

REFERENCES

1) Eaton, W.A., and Hofrichterr, J. 1981. *Methods in Enzymology* **76**: 175-261.
2) Yonetani, T., Iizuka, T., and Waterman, M. R. 1971 *J. Biol. Chem.* **246**: 7683-7689.
3) Asher, S.A. and Shuster, T.M. 1979 *Biochemistry* **18**:5377-5387.
4) Teng, T.Y., Srayer, V., and Moffat, K. 1994 *Nature Struct. Biol.* **1**:701-705.
5) Hartmann, H., Zinser, S., Komninos, P., Schneider, R.T., Nienhaus, G.U. and Parak, F. 1996 *Proc. Natl. Acad. Sci. USA* **93**:7013-7016.
6) Winick, H., and Doniach, S. eds. 1980 Synchrotron Radiation Research. (New York: Plenum)
7) Koch, E.E. ed. 1983-1991 Handbook on Synchrotron Radiation vol. 1-4 (Amsterdam: Elsevier)
8) Wilson, K.S. 1998 *Nature Struct. Biol.* **5**:627-630.
9) Koningsberger, D.C., Prinz, R. 1989 X-ray absorption: principles, applications, techniques of EXAFS, SEXAFS and XANES, John Wiley & Sons, New York
10) George G.N., Hedman, B. and Hodgson, K. 1998 *Nature Struct. Biol.* **5**:645-647
11) Hasnain, S.S., and Hodgson, K. O. 1999. *J. Synchrotron Rad.* **6**, 852-864
12) Yachandra, V., (1995) *Methods in Enzymology*, **246**: 638-675
13) Pin, S., Alpert, B., Congiu Castellano, A., Della Longa, S., and Bianconi, A. 1994 *Methods in Enzymology* **232** 266-292
14) Boffi, A., Das, T.K., Della Longa, S., Spagnuolo, C., and Rousseau, D.L. 1999 *Biophys. J.* **77**:1143-1149
15) Della Longa, S., Pin, S., Cortes, R., Soldatov, A. V., and Alpert, B. 1998 *Biophys. J.* **75** 3154-3162
16) Vojtechovsky, J., Berendzen, J., Chu, K., Schlichting, I., and Sweet, R.M. 1998, PDB code: 1A6K.
17) Popov, A.N., Kachalova, G.S., and Bartunik, H.D. 1998, PDB code 1BZ6
18) Parak, F., Hartmann, H., Aumann, K.D., Reuscher, H., Rennekamp, G., Bartunik, H., and Steigemann, W. 1987 *Eur Biophys J* **15**:237-249
19) Frauenfelder, H., Parak, F., and Young, R.D. 1988 *Ann Rev Biophys Biophys Chem* **17**:451-479
20) Doster, W., Kusack, S., and Petry, W. 1989. *Nature* **337**:754-756
21) Ansari, A., Berendzen, J., Braunstein, D., Cowen, B.R., Frauenfelder, H., Hong, M.K., Iben, I.E.T., Johnson. B., Ormos, P., Sauke, T.B., Scholl, R., Schulte, A., Steinbach, P.J., Vittitow, J. and Young, R.D. 1987 *Biophysical Chemistry* **26**:337-355
22) Gambacurta, A., Piro, M. C., Coletta, M., Clementi, M.E., Polizio, F., Desideri, A., Santucci, R., and Ascoli, F. 1995 *J. Mol. Biol.* **248**:910-917
23) Della Longa, S., Gambacurta, A., Bertollini, A., Girasole, M., Congiu Castellano, A., and Ascoli, F. 2001 *Eur. Biophys. J.* **29**:559-568.
24) Tyson, T.A., Hodgson, K.O., Natoli, C.R., & Benfatto, M. 1992 *Phys. Rev.* **B46**, 5997-6019
25) Binsted, N. & Hasnain, S.S. 1996 *J. Synchrotron Rad.* **3**, 185-196
26) Durham, P., Pendry, J.B., and Hodges, C.H. 1982 *Comput. Phys. Commun.* **25**, 193-200
27) Natoli, C.R., and Benfatto, M. 1986 *J. Phys.* (France) Colloq. **47**, C8:11-23
28) Michalowicz, and A., Vlaic, G. 1998 *J. Synchrotron Rad.* **6**, 1317-1320.
29) Filipponi, A., and Di Cicco, A. 1995. *Phys. Rev.* **B52**, 15135-15144
30) Benfatto, M. and Della Longa, S. 2001 *J. Synchrotron Rad.* **8**, 1087-1094
31) Rehr, J.J., and Albers, R.C. 2000 *Rev. Mod, Phys.* **72**, 621-654
32) Natoli, C.R., Benfatto, M. Della Longa, S., and Hatada, K. 2002 *J. Synchrotron Rad*. in the press
33) Slater, J.C. 1975 *Phys. Rev*. **B10** 3027-****
34) Hedin, L., and Lundqvist, S. 1969. *Solid State Phys*. **23**, 1-15.
35) Hedin, L., and Lundqvist, S. 1971. *J. Phys*. **C4**, 2064-2075
36) Penn, D.R. 1987 *Phys. Rev.* **B35**:482-486.
37) Taylor, J.R. 1972 Scattering Theory . R.E. Krieger Publ. Company, inc Krieger drive, Malabar Florida 32950
38) McKale, A.G., Veal, B.W., Paulikas, A.P., Chan, S.K. and Knapp, G.S. 1988 J. Am. Chem. Soc. 110:3763-3768.

39) James, F., 1994 Cern program library Long Writeup D506. WEB address: http://wwwinfo.cern.ch.asdoc.minuit
40) Chou, S.H., Rehr, J.J., Stern, E.A., Davidson, E.R. 1987. *Phys. Rev*. **B35**, 2604-2614
41) Benfatto, M., D' Angelo, P., Della Longa, S., and Pavel, N.V. 2002 Phys.Rev B, in the press.
42) D' Angelo, P., Benfatto, M., Della Longa, S., and Pavel, N.V 2002 Phys.Rev B, submitted.
43) Benfatto, M., and Felici, R. 2001 *Phys. Rev* **B64** , 115410-9 (2001).
44) Bianconi, A., Congiu Castellano, A., Durham, P.J., Hasnain, S.S., & Phillips, S. (1985) *Nature* **318**, 685-687
45) Petsko, G.A. 1994 *Nature* **371**, 740-741.
46) Schlichting, I., Berendzen, J., Phillips, G.N. Jr & Sweet, R.M. 1994. *Crystal structure of photolysed carbonmonoxy-myoglobin. Nature* **371**, 808-812
47) Vitkup, D., Petsko, G.A. & Karplus, M. 1997. *A comparison between molecular dynamics and X-ray results for dissociated CO in myoglobin. Nat. Struct. Biol.* **4**, 202-208
48) Teng, T.-Y., Srajer, V. & Moffat, K. (1997). *Initial trajectory of carbon monoxide after photodissociation from myoglobin t cryogenic temperature. Biochemistry* **36**, 12087-12100. PDB codes: 1AJG, 1AJH
49) Meller, J. & Elber, R. 1998 *Biophys. J.* **74**:789-802
50) Chu, K., Vojtchovsky, J., McMahon, B.H., Sweet, R.M., Berendzen, J. & Schlichting, I. 2000 *Nature* **403**, 921-923
51) Kachalova, G.S., Popov, A.N. & Bartunik, H.D. 1999. *Science* **284**, 473-476 . PDB codes: 1BZP, 1BZR
52) Vojtechovsky J., Chu K., Berendzen J., Sweet R.M. & Schlichting I.. 1999 *Biophys. J.* 77, 2153-2174. PDB codes: 1A6G,1A6K,1A6N
53) Iizuka, T., Yamamoto, H., Kotani, M. & Yonetani, T. 1974 Low temperature photodissociation of hemoproteins: carbon monoxide complex of myoglobin and hemoglobin. *Biochim. Biophys. Acta* **371**, 126-139
54) Della Longa, S., Arcovito, A., Vallone, B., Congiu Castellano, A., Kahn, R., Vicat, J., Soldo, Y. & Hazemann, J.L. 1999 *J. Synchrotron Rad.* **6**, 1138-1147
55) Powers, L., Chance, B., Chance, M., Campbell, B., Khalid, J., Kumar, C., Naqui, A., Reddy, K.S. & Zhou, Y. 1987 *Kinetic, structural and spectroscopic identification of geminate states of Mb: a ligand binding site of reaction pathway. Biochemistry* **26**, 4785-4796
56) Della Longa, S., Arcovito, A., Girasole, M., Hazemann, J.L., & Benfatto M. 2001 *Phys. Rev. Lett.* **87**, 155501-04.
57) Pedio, M., Benfatto, M., Aminpirooz, S., Haase, J. 1994 *Phys. Rev*. **B** 50, 6596-6602
58) Díaz-Moreno, S., Muñoz-Páez, A. & Chaboy, J. 2000 *J. Phys. Chem.* A **104**, 1278-1286
59) Kuriyan, J., Wilz, S., Karplus, M. & Petsko, G.A. 1986. X-ray structure and refinement of Carbon-monoxy (Fe II)-myoglobin at 1.5 Å resolution. *J Mol Biol* **192**, 133-154. PDB code: 1MBC.
60) Cruickshank, D.W.J. 1999 *Acta Cryst.* **D55**, 583-601
61) Ostermann, A., Waschipky, R., Parak, F., and Nienhaus, G.U. 2000 *Nature* **404**:205-208.
62) Lim, M., Jackson, T.A., and Anfinrud, P.A. 1995 *Science* **269**:962-966
63) Sage, J.T., and Jee W. 1997 *J Mol Biol* **274**:21-26